WASHINGTON
UNIVERSITY
IN ST. LOUIS

(NASA-CR-155250) IMAGING NATURAL MATERIALS WITH A QUASI-MICROSCOPE Final Report, 1 Jul. 1974 - 31 Aug. 1977 (Washington Univ.) 47 p HC A03/MF A01 CSCL 20F

N78-11813

Unclas
G3/74 52828

McDonnell Center For the Space Sciences

IMAGING NATURAL MATERIALS WITH A QUASI-MICROSCOPE

Susan Bragg and Raymond Arvidson
McDonnell Center for the Space Sciences
Department of Earth and Planetary Sciences
Washington University
St. Louis, Missouri 63130

Final Contractor's Report

NASA Langley Research Center Study Contract
NSG-1084
July 1, 1974 - August 31, 1977

IMAGING NATURAL MATERIALS WITH A QUASI-MICROSCOPE

Susan Bragg and Raymond Arvidson
McDonnell Center for the Space Sciences
Department of Earth and Planetary Sciences
Washington University
St. Louis, Missouri 63130

Final Contractor's Report

NASA Langley Research Center Study Contract
NSG-1084
July 1, 1974 - August 31, 1977

TABLE OF CONTENTS

1. INTRODUCTION

This report is a summary of work carried out under a study contract with the Flight Instrumentation Division (FID) of the NASA Langley Research Center. The study was concerned with evaluating the scientific potential of a breadboard quasi-microscope (QM) built for FID by the Perkin Elmer Corporation. The flight-configured QM, as presently planned, would consist of the Viking lander camera, with auxiliary optics mounted inside the dust post (Figure 1). During mission operations, prepared samples would be delivered to a plate positioned within the QM field of view and depth of focus. The auxiliary optics would then allow soil samples to be imaged with an 11 μm pixel size in the broad band (high resolution, black and white) mode, and a 33 μm pixel size in the multispectral mode. Other details as to QM size, depth of focus, etc., are given in Table 1.

A pixel size of 10-30 μm would be a vast improvement in resolution over either the lunar Surveyor cameras, the Mars Viking lander cameras, or the Venus Venera imaging system. Each of the Surveyors that soft-landed on the moon in the 1960's was equipped with a TV camera that, in near field, could resolve objects as small as 0.5 mm (Jaffe,1969). The four Viking lander cameras operating on Mars have resolved soil texture in the near field at a resolution of somewhat less than 1 cm. (Mutch, et al, 1976 a,b,c). Finally, the Venera system has shown a capability to resolve objects a few centimeters across (Florensky et al, 1977). Unfortunately, a significant fraction of the particles composing the soils on these three planets is below the resolving power of the imaging systems. This has resulted in a lack of critical information about soils, namely: (1) the size distribution of grains produced by igneous (intrusive and extrusive) processes or by shock metamorphism, (2) the size distribution resulting from crushing, chemical alteration, or by hydraulic or aerodynamic sorting, (3) the shape and degree of grain roundness and surface texture induced by mechanical and chemical alteration, and (4) the mineralogy and chemistry of grains. Research reported in this report has been directed toward determining the utility of a quasi-microscope, as presently designed, to characterize these parameters. Our analyses have been limited to the range and quality of information that can be obtained about the inorganic characteristics of soils; it should be noted that the concept also has definite biologic applications. Finally, the term soil is not meant to conote biologic processes, but rather as a descriptive term for particulate materials.

2. DISCUSSION OF APPROACH

Our approach has been to select a limited number of samples that display a range of grain sizes, shapes, surface textures,and mineralogies. Eight samples: three crystalline igneous rocks (latite, basalt, peridotite), four volcanic tuffs, and a limonite sample, were chosen to fulfill these requirements. The samples were disaggregated, seived, and examined under a Zeiss petrographic microscope to provide ground truth observations for comparison with QM data. Details as to sample petrography are given in Appendix I. The samples were then imaged with the QM assembly and with the Zeiss microscope. The photographs are shown in Appendix II, along with brief descriptions as to the nature and quality of information that can be extracted from each frame. Appendix III has, for reference, spectral reflectance data for the .4-1.1 μm wavelength region, for each of the samples, together with a number of other samples that were examined during the course of research. In the following sections, based on comparison of ground truth observations of the samples with QM images, we evaluate the utility of the QM and we make recommendations as to design criteria that should be met for future breadboard and flight-configured microscopes.

We should note that our approach assumes use of a QM or similar instrument on board a lander in a relatively simple way - delivery of a prepared sample and imaging under reflected light. Previous design concepts for microscope assemblies called for complex and costly mechanisms (transmitted light, polarization filters, sandwiching grains between plastic sheets, etc.) that duplicated classical methods of microscopic petrography (Loomis, 1965). Our results indicate that reflected light is suitable for characterizing grain size, shape, and surface texture, and that multispectral imaging in the visible and reflected IR is sufficient to characterize grain mineralogy, at least to first order. A lighting angle of approximately 45^{0} inclination from the sample surface appears to be optimum for textural studies, while a near-normal illumination is best for characterizing grain spectrophotometric properties.

3. CHARACTERIZATION OF SIZE, SHAPE, ROUNDNESS, AND SURFACE TEXTURE OF GRAINS

Appendix II contains a detailed comparison of QM and high-quality Zeiss petrographic microscope photographs. The petrographic scope has a nominal resolving power of about 3 μm at 50% MTF. The QM has a pixel size of 11 μm for the high resolution mode, and a 33 μm pixel size for the multispectral mode.

High resolution QM pictures are sufficient to accurately determine particle sizes for grains ≥100 μm. Grains smaller than this are difficult to resolve as discrete particles. The upper limit for determining grain size is, of course, a function of depth of focus. The largest grains examined, which were 250 μm, were quite accurately represented in terms of grain size. The QM multispectral mode, on the other hand, is practically useless for estimation of particle size, since grain edges usually cannot be delineated.

Two parameters that are of use in understanding the history of mechanical abrasion, chemical weathering, and other alteration processes for soils, are grain shape and roundness. Both can be expressed as a Fourier series in polar coordinates as follows:

$$R(\theta) = R_0 + \sum_{i=1}^{N} R_i \cos (i\theta - \phi_i) \qquad (1)$$

where the expression is a Fourier series, with $R(\theta)$ as the radius from the center of gravity to the periphery of a grain as seen in either the Zeiss or QM view, in a direction, θ. R_0 is the mean radius from the center of area to the grain periphery, R_i is the amplitude and ϕ_i is the phase angle for the ith harmonic (Ehrlich and Weinberg, 1970).

Particle shape has traditionally been measured in terms of degree of deviation from a sphere. With expression (1), shape information would be contained in the first several harmonics. Examination of the QM high resolution pictures in Appendix II shows that, for grain sizes ≥100 μm, shape information could be readily determined.

Grain roundness is a much more meaningful measurement than is grain shape. Shape is usually an inherited property, that is, the shape of a grain in terrestrial sediments is strongly dependent on crystal cleavage patterns, and the

manner in which the grain grew and the manner in which it weathered from crystalline rock (Blatt et al, 1972). As an example, note the distinct cleavage patterns for the pyroxenes shown in Figures II-3 and II-4. Roundness, on the other hand, describes the sharpness of the corners and edges of a grain. Roundness is much more sensitive to the conditions of mechanical and chemical weathering and erosion from the time period when the grain was first weathered from a crystalline rock to the time it was incorporated as a sediment. With equation (1), roundness information would be contained in higher order harmonics, typically 5th order and higher.

Examination of the high resolution QM views shows that most of the grain roundness detail is preserved, except for very high order terms, such as the tenth and higher harmonics. QM color views, on the other hand, provide little or no information on grain roundness properties.

In summary, for the grain sizes examined, QM high resolution views provide acceptable quality for determining grain size, shape, and roundness for particles $\geq$ 100 μm. For smaller particles, roundness information cannot be obtained and grain shape and size is severely compromised. For larger particles, the limiting factor is the depth of focus.

The one important characteristic that is lost even on the QM high resolution views is grain surface texture. For instance, note the abundance of spalled (fractured) zones due to crushing visible on the Zeiss views in Figures II-5, and the small grain aggregates clinging to larger grains in Figures II-7, 8, 9, and 11. Very little of this information is accurately portrayed in the QM views, because of the inherently lower resolution. Stereo viewing using the quasi-microscope (Burcher, et al, 1977b) alleviates this problem somewhat by providing a means for three dimensional viewing of grain surfaces. However, the fundamental limitation is the 11 μm spot size, combined with the QM MTF. Most surface texture for terrestrial materials, such as spall zones, pits, grooves, striations, comes in sizes smaller than the QM high resolution spot size.

4. MULTISPECTRAL IMAGING AND THE POTENTIAL FOR CHARACTERIZING MINERALOGY OF GRAINS

Four of the samples (limonite, basalt, peridotite, tuff-3) were imaged in color with the QM. Two of the samples (limonite, tuff-3) were also successfully imaged in the reflected infrared. The FID camera has six (bandwidth=.1 μm) channels, the three in the color are centered at about .45 μm, .55 μm, and .65 μm, while the three IR channels are centered at 0.80 μm, 0.90 μm, and 1.0 μm. The six-channel images of the limonite and tuff-3 were taken in sequence with calibration images of a neutral gray surface with an 18% reflectance. A number of other 6-channel images of other samples were acquired with the FID camera at NASA Langley, using a heliostat. However, that data has turned out to be rather useless because passing clouds significantly changed the illumination characteristics between the time soils were imaged and pictures were acquired of the gray calibration surface. The successful color and IR data were acquired with a tungsten lamp illumination source. The images acquired are given in Table II.

Examination of the QM color images in Appendix II clearly shows the effect of decreasing resolution from an 11 μm pixel size to a 33 μm pixel size. Grain edges are blurred, although color differences between grains can still be seen. For the limonite and volcanic tuff-3, an attempt was made to construct a reflectance spectrum in the wavelength range covered by the FID channels, ~.4-1.1 μm. Spectra, which are necessarily undersampled estimates, since only 6 samples were acquired over 0.7 μm, were generated by delineating individual grains on the color images. DN values were then obtained for the region occupied by the grains and averaged. Reflectance for each grain, relative to the neutral gray chart, was then computed as follows:

$$\rho(\lambda) = \frac{\overline{DN}\ \text{grain}}{\overline{DN}\ \text{chart}} \Big/ \frac{\text{Gain grain}}{\text{Gain chart}} \qquad (2)$$

where $\rho(\lambda)$ is the approximation of the grain's reflectance at the center wavelength of each of the channels and gain refers to the gain setting for the camera.

Results for these computations, overlain onto Cary 14 ground truth spectra are shown in Figure 2. Results are very disappointing. First, limonite is fairly monomineralic, so that spectra should be constant from place to place. Thus, using a microscope to examine individual grains in a multispectral mode provides little additional mineralogical information. Second, for the volcanic tuff-3, the grains examined appear to have spectra that are similar to the average spectra for the sample,

i.e. the Cary 14 spectra. The reason for this is not known since the QM color view (Figure II-2) shows definite differences between the mafic minerals and the brighter feldspars. Unfortunately, decipherable six channel data do not exist for the one sample (basalt) that probably would have allowed us to demonstrate that a soil spectrum can be deconvolved into its mineralogic components by use of multispectral imaging through a microscope.

Some discussion and breadboard design for future planetary lander cameras has involved augmenting the present 6-channel Viking lander camera system (silicon photo diodes) with PbS diodes (Kelly, 1975). The PbS diodes, which would be used in a spectrometer mode, would extend the spectral coverage out to about 2.5 μm. To test the utility of such spectral curves we have run some simulations of the camera's ability to generate reflectance estimates of probable Martian materials with Si and PbS detectors. Four samples were chosen for the simulations, based on the presence of a variety of spectral features. The materials are a limonite, hypersthene, augite, and an olivine (Figure 3). Perhaps the most outstanding feature of the limonite spectrum is the broad absorption feature centered at .89 μm. This feature is an Fe^{+3} electronic transition band (Adams, 1975). Narrow bands at 1.4 and 1.9 μm are vibrational bands due to H_2O and OH^- in the limonite crystal lattice (Hunt and Salisbury, 1970). The two pyroxenes, hypersthene and augite, dominate spectral properties of olivine-poor basalts (Adams, 1974). Hypersthene has broad bands centered at 0.895 μm, and at 1.817 μm, while augite has bands at 0.95 μm, and at 2.09 μm. The exact location of the pair of bands near 1 and 2 μm serves to uniquely distinguish between the two pyroxenes. The absorptions are Fe^{+2} electronic transitions features. Olivine has a Fe^{+2} electronic transition band at 1.0 μm, but it lacks the band near 2.0 μm common to pyroxenes. Accurate reproduction of the spectra of these minerals would allow positive identification, based on the location and breadth of the absorption bands. Accurate reproduction of band depths, in addition to locations and breadths, allows estimation of the abundances of minerals to be made (Gaffey, 1976).

The fundamental performance and design parameters for using the Viking lander cameras as radiometers are contained in the signal to noise expression for a given channel:

$$S/N = .156\ \beta^{3/2} \int_0^{\infty} S(\lambda)\ T_a(\lambda)\ T_c(\lambda)\ T_f(\lambda)\ D_*(\lambda)\ \rho(\lambda)\ d\lambda \quad (3)$$

where: β= instantaneous camera field of view, which is 0.12 degrees, $S(\lambda)$ = solar irradiance above the atmosphere, $T_a(\lambda)$ is the atmospheric transmittance,

$T_c(\lambda)$ is the transmittance of the camera optics, $T_f(\lambda)$ is the filter transmittance, $D_\lambda(\lambda)$ is the photodiode detectivity, and $\rho(\lambda)$ is the spectral reflectance of the surface (Kelly, 1975).

The factors which influence the correct placement, number, and width of the filters for the system are a function of camera variables, scene variables, and design constraints. Design constraints force selection of the minimum number of possible channels to maintain electronics simplicity. The number and center wavelengths of the filters should, however, be driven by the spectral reflectance of the materials being considered. The curve representing olivine illustrates a slowly varying reflectance; there is one band in the IR, which is quite broad. The limonite, however, is a curve with both broad and narrow features. To reproduce the narrow water bands it is necessary to sample the curve at twice the highest frequency in those regions, according to the Nyquist sampling theory. This corresponds to placing the center of one channel at the bottom, and one channel each on the shoulders of the bands.

Limonite was used to force placement of channel center wavelengths, since its spectra is the most complex. Channel bandwidth can be computed once the center wavelength is chosen, since bandwidth can be shown to be a function of wavelength. Let the filter transmittance function be Gaussian in nature and let the maximum transmittance of the filter be 0.5. The width of the filter transmittance can be described by its standard deviation, σ. The filter transmittance can be represented by:

$$T(\lambda)_f = 0.5 \exp\left[\frac{-(\lambda-\mu)^2}{2\sigma^2}\right] \qquad (4)$$

Substituting the right hand portion of equation (4) for the variable $T_f(\lambda)$ in equation (3) then allows a solution for the standard deviation, σ, as a function of filter center wavelength, μ, when a S/N = 256 is used for $\rho(\lambda) = 1.0$. Filter center wavelengths were selected based on quantifying broad and narrow absorption features in Figure 3, using the Nyquist sampling theorem. With selection of a center wavelength, filter spread, σ, was then computed. Results are given in Table III.

The response of the camera system to any given $\rho(\lambda)$ can be simulated by inputting a given $\rho(\lambda)$ for each channel and computing S/N, and then normalizing that result to S/N = 256, i.e. a $\rho(\lambda) = 1.0$ (Kelly, 1975). Results for simulations of limonite, hypersthene, augite, and olivine, are shown in Figure 3. None of the spectra are

accurately represented by the system designed for limonite. First, the PbS channels placed to detect the water bands for limonite are too broad to accurately reproduce the depths of these narrow absorption features. Second, 12 channels are not sufficient to reproduce all four spectra. For instance, it is doubtful that the subtle, yet important, shifts in maximum absorption near 1.0 μm for the hypersthene, augite, and olivine, could be reproduced. Clearly, if a system is to be flown on a future lander, it would be very desireable to be able to identify minerals by their diagnostic absorptions. Many more channels, and narrow channels in the longer wavelengths, are needed to perform that job. As an example of a very ambitious, but nonetheless scientifically important system, the Lunar Polar Orbiter has on board a 256 channel spectrometer that covers the wavelength range from .4 to 2.5 μm (LPO Mission Summary, 1976).

SUMMARY AND RECOMMENDATIONS

1. The bread board quasimicroscope (QM), used in the high resolution mode (11 μm pixel size), is capable of resolving grain sizes and shapes for grain sizes ≥100 μm. Grain surface textures, such as spall zones, pits, grooves, are not reproduced by the QM, mainly because the characteristic sizes of these features fall below 10 μm.

2. QM color views, with a 33 μm pixel size, do not portray correct grain sizes, shapes, or degree of roundness for grains in the size range from 77 to 250 μm. In most cases, grain edges cannot be resolved. Color differences do serve to characterize sample heterogeneity and the differences in most cases are readily interpretable as indicative of varying mineralogy. Color imaging with a minimum pixel size of 11 μm is highly desireable.

3. QM 6-channel multispectral data (.4 - 1.1 μm) for limonite and a volcanic tuff indicate that reflectance spectra for individual grains can be estimated. For soils with a number of mineral phases, the potential exists for being able to deconvolve a reflectance spectrum into components by examining spectra of single grains under the QM. However, the severe undersampling of spectral features with 6-channels over 0.7 μm would hamper positive identification of most minerals, based on the depth, breadth, and location of absorption features (Huck et al, 1977b).

4. Augmentation of a Viking - QM camera system with PbS channels is strongly recommended, since much diagnostic information of mineral content can be found in the 1.0 - 2.5 μm range covered by PbS diodes. A 12-channel (.4-2.5 μm) system using silicon and PbS diodes was simulated in this study and the capability to uniquely identify four minerals was evaluated. Results are fairly negative: diagnostic absorption features in the .4 - 2.5 μm range that allow characterization of minerals are either to narrow (water bands) or shift too little (Fe^{+2} bands due to hypersthene - augite - olivine) to be accurately represented by a 12 channel system. More channels over the entire wavelength range, and narrower channels in the PbS range, are needed.

5. Finally, we note that the QM, if it advances to the stage of a flight instrument on a planetary lander, should be used as part of a package of instruments that are designed to characterize soil size distribution, particle shape, roundness, chemistry, and mineralogy. The QM, with high spatial resolution color imaging, and with high spectral resolution characterization in the .4 - 2.5 μm range, would be an extremely valuable link in a system of: (a) sample acquisition (b) sample preparation, (c) sample examination (with QM), and (d) sample analysis by more sophisticated means, such as X-ray fluorescence, diffractometry, etc. Such a system was, in fact, recommended by a number of members of the Mars 1984 Rover Science Working Group (MSWG Report, 1977). Color imaging at an 11 μm pixel size is a minimumly acceptable design only if sample preparation involves removal of grain sizes $\leq$ 100 μm. High spectral resolution can be obtained by divorcing imaging from spectral characterization. Interesting areas, seen on color QM views, could be examined with a multi-channel "single pixel" spectrometer to save on data allocations. The number, bandwidths and locations of the channels should be selected to characterize the range of materials likely to be encountered during the course of the mission.

ACKNOWLEDGEMENTS

Thanks are given to members of FID, NASA Langley (F. Huck, E. Burcher, L.Kelly, S. Wall, and others) for helping us in various phases of this study. Charlene Ehll spent a great deal of time in manuscript preparation, always in a cheerful mode. E. Guinness, D. Chervitz, and J. Reed provided needed technical assistance. This report constitutes the final contractural obligations for NASA Langley Study Contract # NSG-1084 to Washington University.

REFERENCES CITED

Adams, J., 1975, Interpretation of Visible and IR Diffuse Reflectance Spectra of Pyroxenes and Other Rock-forming Minerals, IR and Raman Spectroscopy of Lunar and Terrestrial Minerals, C. Karr, ed., Academic Press, pp. 91-116.

Adams, J., 1974, Visible and Near-IR Diffuse Reflectance Spectra of Pyroxenes as Applied to Remote Sensing of Solid Objects in the Solar System, Journal of Geophysical Research, V. 79, pp. 4829-4836.

Arvidson, R. and Mutch, T., 1974, Sedimentary Patterns in and around Craters from the Pinacate Volcanic Field, Sonora, Mexico, Geological Society of America Bulletin, V. 85, pp.99-104.

Blatt, H., Middleton, G., Murray, R., 1972, Origin of Sedimentary Rocks, Prentice Hall, 634 pp.

Burcher, E., Huck, F., Wall, S., Bragg, S., 1977, Performance Evaluation of a Quasi-microscope for Planetary Landers, NASA Technical Note D-8370, 23 pp.

Burcher, E., Sinclair, A., Huck, F., 1977, Quasimicroscope Concept for Planetary Missions: Stereo, submitted to Applied Optics.

Burns, R. and Vaughn, D., 1975, Polarized Electronic Spectra, in IR and Raman Spectroscopy of Lunar and Terrestrial Minerals, C. Karr, ed., Academic Press, pp. 39-72.

Ehrlich, R. and Weinberg, B., 1970, An Exact Method for Characterization of Grain Shape, Journal of Sedimentary Petrology, V. 40, pp. 205-212.

Florensky, C., and others, 1977, The Surface of Venus as Revealed by Soviet Venera 9 and 10, Geological Society of America Bulletin, V. 88, pp. 1537-1545.

Gaffey, M., 1976, Spectral Reflectance Characteristics of Meteorite Classes, Journal of Geophysical Research, V. 81, pp. 905-920.

Huck, F., Arvidson, R., Burcher, E., Giat, O., Wall, S., 1977, Quasi-microscope Concept for Planetary Missions, Applied Optics, V. 16, p. 2454-2459.

Huck, F. , Jobson, D., Park, S., Wall, S., Arvidson, R., Patterson, W., 1977, Spectrophotometric and Color Estimates of the Viking Lander Sites, Journal of Geophysical Research, V. 82, pp. 4401-4411.

Hunt, G., Salisbury, J., 1970, Visible and Near-IR Spectra of Minerals and Rocks: 1. Silicate Minerals, Modern Geology, V. 1, pp. 283-300.

Jaffe, L.D., 1969, The Surveyor Lunar Landings, Science, V. 164, pp. 775-788.

Kelly, W. L., 1975, Investigation of Facsimile Camera-spectrometer Capability in the 1.0 to 2.7 Micron Spectral Range, NASA Technical Memo X-72714, 18 pp.

Loomis, A., 1965, A Lunar and Planetary Petrography Experiment, NASA Technical Report 32-785, 22 pp.

Mars Science Working Group, 1977, A Mars 1984 Mission, NASA Technical Memo 78419.

Mission Summary for Lunar Polar Orbiter, 1977, JPL Document 660-41, Rev A, 22 pp.

Mutch, T.A., Arvidson, R.E., Binder, A.B., Huck, F.O., Levinthal, E.C., Liebes, S., Morris, E.C., Nummedal, D., Pollack, J.B., Sagan, C., 1976, Fine Particles on Mars: Observations with the Viking Lander 1 Cameras, Science, V. 194, pp. 87-91.

Mutch, T.A., Binder, A.B., Huck, F.O., Levinthal, E.C., Liebes, S., Morris, E.C., Patterson, W.R., Pollack, J.B., Sagan, C., Taylor, G.R., 1976, The Surface of Mars: The View from Viking Lander 1, Science,V. 193, pp. 791-801.

Mutch, T.A., Grenander, S.U., Jones, K.L., Patterson, W., Arvidson, R.E., Guinness, E.A., Avrin, P., Carlston, C.E., Binder, A.B., Sagan, C., Dunham, E.W., Fox, P.L., Pieri, D.C., Huck, F.O., Rowland, C.W., Taylor, G.R., Wall, S.D., Kahn, R., Levinthal, E.C., Liebes, S., Tucker, R.B., Morris, E.C., Pollack, J.B., Saunders, R.S., Wolf, M.R., 1976, The Surface of Mars: The View from Viking Lander 2, Science, V. 194, pp. 1277-1283.

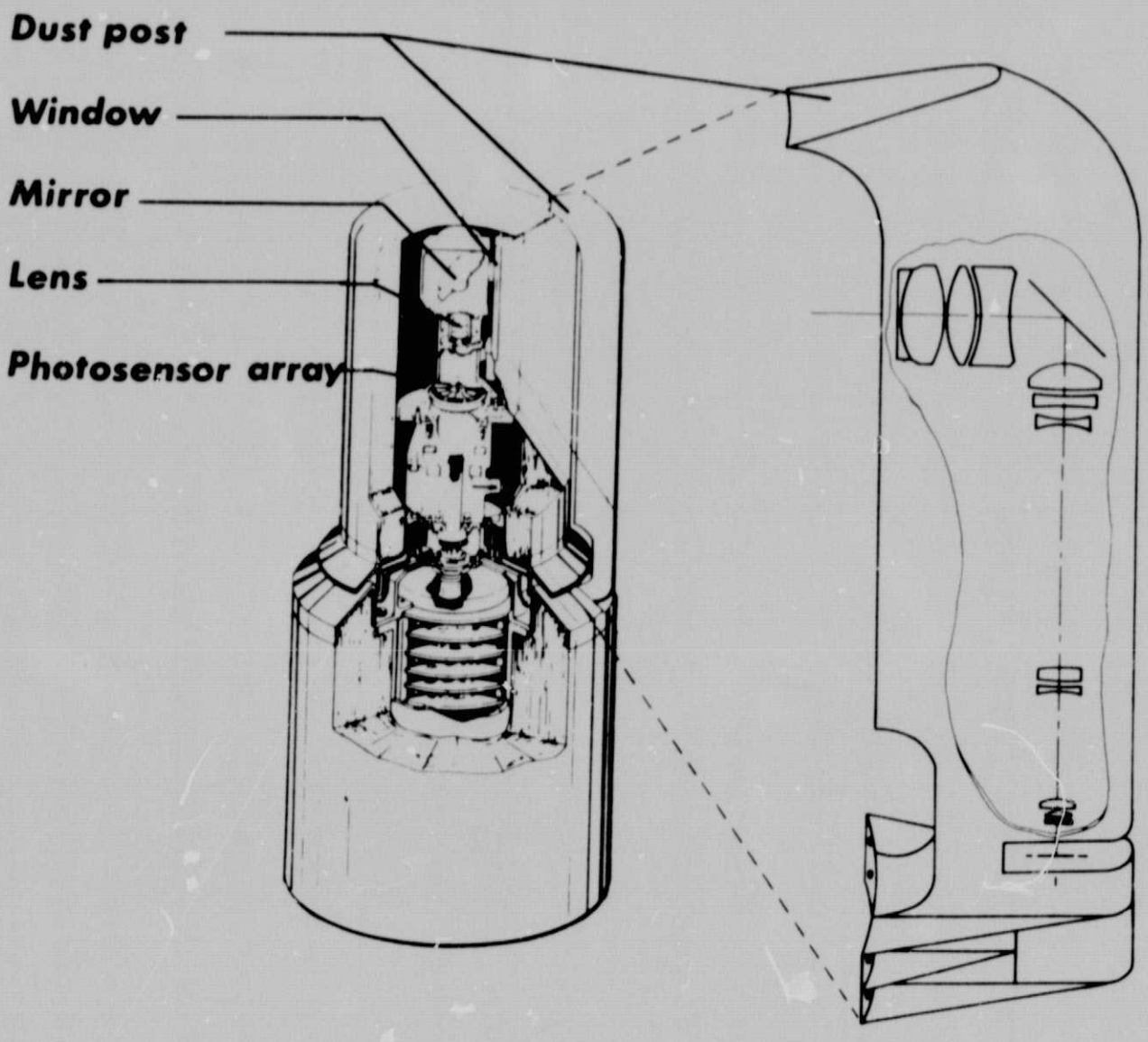

Figure 1. - Simplified cutaway view of Viking lander camera with quasi-microscope optics. It is assumed in this analysis that soil samples would be delivered to a plate mounted at the base of the dust cover, for imaging with the quasi-microscope. After Huck et al, 1977

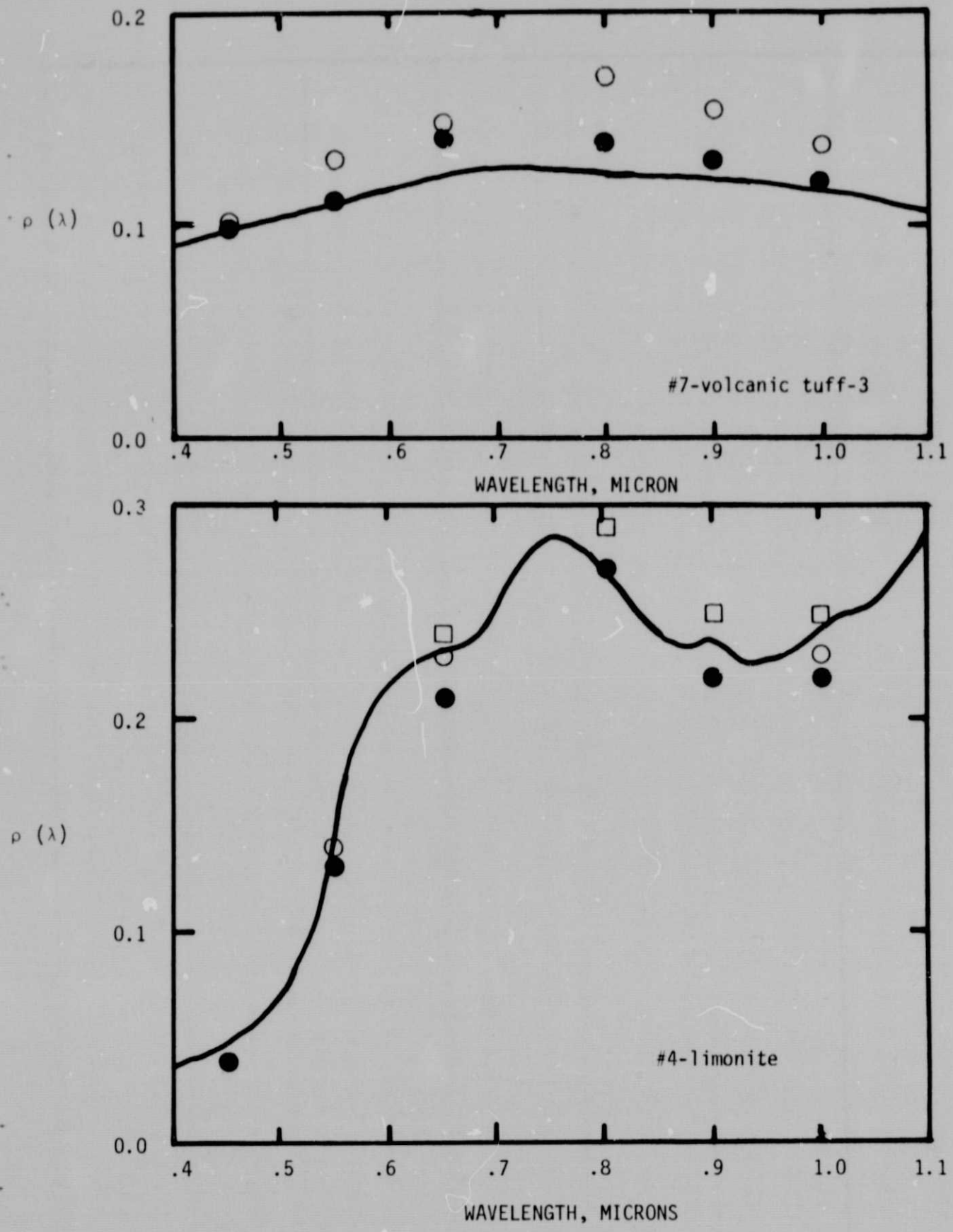

Figure 2: Solid lines are Cary-14 ground truth spectra. Points are 6-channel spectra for individual grains seen in QM color and IR views. For Sample #7, open circles are for a light grain and dark circles are for a dark grain.

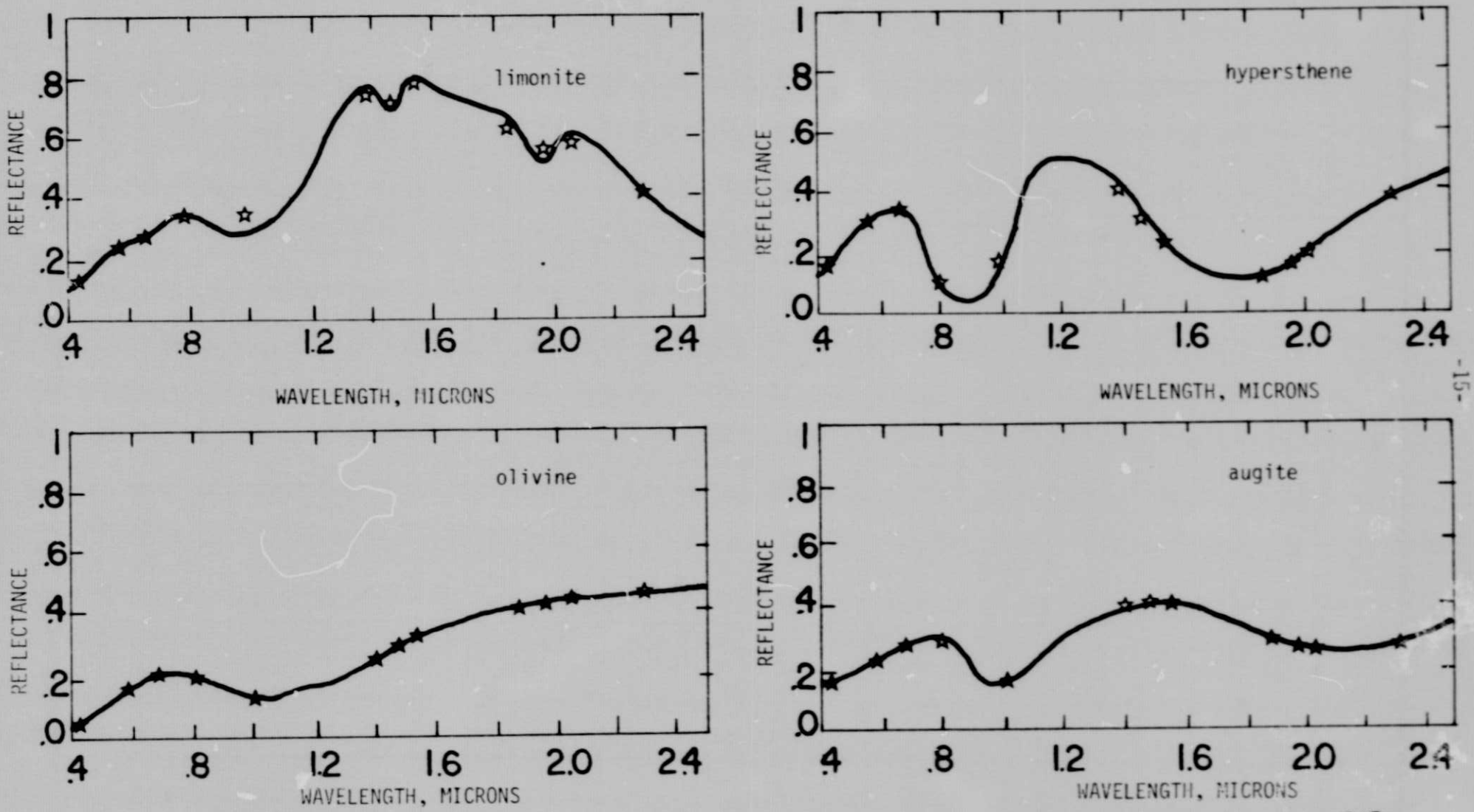

Figure 3: Solid lines are true spectra, while stars indicate the predicted reflectance with 12-channel Si and PbS detector system. Note the subtle shift in absorption near 1.0 μm for the hypersthene, augite, and olivine. Limonite curve was obtained with the FID Cary-14, using Sample #4. Other curves are from Adams (1974).

TABLE I. QUASI-MICROSCOPE PERFORMANCE PREDICTION BASED ON FIRST-ORDER OPTICAL ANALYSES, AFTER HUCK ET AL 1977.

Performance parameter	Camera imaging mode	
	High-resolution	Multispectral
Diameter of pixel in object field, d, μm	11	33
Geometric resolution, μm/lp	22	66
Geometric depth of field, Δl, μm	32/focus step 128, with four focus steps	96
Diameter of unvignetted object field, mm	4.1	4.1
Number of adjacent contiguous pixels per object field diameter	372	124

TABLE II

List of images acquired with the QM-FID system at NASA Langley Research Center. File and tape numbers indicate FID records. An X under the tape column indicates a tape lost somewhere at FID.

SAMPLE	TAPE	FILE	MODE	LIGHT	PICTURE	DN	COMMENT
#2-Basalt	X	4	High Resolution Single	T	Y	N	
	X	5	High Resolution Double	T	Y	N	
	913802520	11	High Resolution Single	T	Y	N	
	95534	2	Color	S	Y	N	
Grey Card	95534	3	Color	S	N	Y	Used for calibration
	95534	7	IR	S	N	Y	Used for calibration
#1-Latite	913802520	8	High Resolution Single	T	Y	N	
	X	2	High Resolution Single	T	Y	N	
	X	3	High Resolution Double	T	Y	N	
#4-Limonite	913802520	6	High Resolution Single	T	Y	N	
	X	6	High Resolution Single	T	Y	N	
	X	7	High Resolution Double	T	Y	N	
	95534	1	Color	S	Y	N	
	95534	4	Color	S	N	Y	Glue mounted
	95534	8	IR	S	N	Y	Glue mounted
	913802520	16	Color	T	Y	N	
	913802520	17	IR	T	N	N	
	913802520	25	Color	T	Y	Y	Used in spectral reduction, Fig.2
	913802520	26	IR	T	N	Y	Used in spectral reduction, Fig. 2
#30 Loess	913802520	5	High Resolution Single	T	Y	N	
	X	1	High Resolution Single	T	Y	N	
Magnesium Carbonate	913802520	1	High Resolution Single	T	Y	N	
	913802520	23	Color	T	N	Y	Used for calibration, Fig. 2
	913802520	24	IR	T	N	Y	Used for calibration, Fig. 2
#3-Peridotite	913802520	13	High Resolution Single	T	Y	N	
	X	16	High Resolution Single	T	Y	N	
	X	17	High Resolution Double	T	Y	N	
	95534	6	Color	S	Y	Y	DN's not usable, glue mounted
	95534	10	IR	S	N	Y	DN's not usable, glue mounted

TABLE II, cont.

SAMPLE	TAPE	FILE	MODE	LIGHT	PICTURE	DN	COMMENT
#5-Volcanic	913802520	2	High Resolution Single	T	Y	N	
Tuff-1	X	12	High Resolution Single	T	Y	N	
	X	13	High Resolution Double	T	Y	N	
#6-Volcanic	913802520	4	High Resolution Single	T	Y	N	
Tuff-2	X	10	High Resolution Single	T	Y	N	
	X	11	High Reoslution Double	T	Y	N	
#7-Volcanic	913802520	12	High Resolution Single	T	Y	N	
Tuff-3	X	8	High Resolution Single	T	Y	N	
	X	9	High Resolution Double	T	Y	N	
	95534	5	Color	S	N	N	
	95534	9	IR	S	N	N	
	913802520	13	Color	T	N	N	
	913802520	14	IR	T	N	N	
	913802520	28	Color	T	Y	Y	Used in spectral data reduction, Fig. 2
	913802520	29	IR	T	N	Y	Used in spectral data reduction, Fig. 2
#8-Volcanic	913802520	7	High Resolution Single	T	Y	N	
Tuff-4	X	14	High Reoslution Single	T	Y	N	
	X	15	High Resolution Double	T	Y	N	

Y = on file, N = not on file

X = tape number unknown (single tape)

T = Tungsten lamp

S = Sun through heliostat

TABLE III

Summary of locations and breadths of 12-channel silicon and PbS detector system for the Viking Lander camera. Band width is defined as 2.35 times the standard deviation. Large bandwidths at longer wavelengths are needed because the solar flux is very low. With the present camera scanning rate and angular resolution, channels centered over the H_2O bands are too broad to accurately depict these absorptions.

Channel Number	Center Wavelength (μm)	Bandwidth	Standard Deviation
1	0.425	0.0035	0.00149
2	0.575	0.0014	0.00061
3	0.675	0.0016	0.00070
4	0.800	0.0018	0.00079
5	1.000	0.0070	0.00297
6	1.400	0.0617	0.02626
7	1.475	0.0640	0.02723
8	1.550	0.0757	0.03220
9	1.875	0.1004	0.04272
10	1.975	0.1360	0.05787
11	2.075	0.1590	0.06766
12	2.300	0.1913	0.08140

The solar flux used was that expected at 1.52 astronomical units, the location of Mars. Resultant bandwidths are slightly optimistic since the atmospheric transmittance function used assumed a dust-free atmosphere, with transmittance close to unity. Viking Lander camera data show the transmittance is much lower than unity, perhaps closer to 0.65 (and highly variable) due to suspended dust (Mutch et al, 1976a).

APPENDIX I: Description of Samples

A. Eight samples were prepared and photographed both with the quasimicroscope assembly and with a Zeiss petrographic microscope. The results are displayed and described in Appendix II and an evaluation of the information content in the photographs can be found in the main body of the report. Spectral curves for the samples, from .4 to 1.1 μm, are included in Appendix III.

B. Following is a brief description of each sample, stressing the kinds of information obtainable with high-resolution (≈ 3 μm) examination of free grains with reflected light, using a Zeiss binocular petrographic microscope. Where needed, thin sections were made and examined to determine mineral abundances.

1-Latite: This sample consists of a crushed latite, which is an intermediate-composition volcanic rock. Size fraction used in the studies was 74-250 μm. Latite consists of about 65% (by grain count) plagioclase feldspar, together with clinopyroxene (20% by grain count), minor olivine, and various opaque and accessory minerals.

2-Basalt: The sample was synthesized by mixing equal weight fractions of crushed augite, hypersthene, and labradorite. The mineral phase abundances were chosen so as to mimic a norite, which is a common lunar basalt type. Size interval used in studies was 177-250 μm.

3-Peridotite: The sample consists of a crushed peridotite, an ultrabasic (Fe, Mg-rich) igneous rock consisting dominanatly of augite (85% by grain count), with the remainder being olivine and hypersthene. Size interval used was 74-125 μm. (Samples 1, 2, and 3 were chosen to represent a variety of mineral phases found in igneous rocks.)

4-Limonite: The sample consists of crushed limonite, an iron hydroxide weathering product of Fe-rich minerals. The sample contains a few percent (by grain count) of quartz and potash feldspar grains. Size fraction used is 77-125 μm.

5-Volcanic Tuff-1: The sample consists of volcanic ash collected from the tuff breccias exposed on the walls of MacDougal Crater, Pinacates volcanic field, Sonora, Mexico. The sample was sieved and the 177-250 μm size fraction was

used. Quartz, potash feldspar, and plagioclase feldspar 85% (by grain count) of the sample. Opaque minerals and metamorphic rock fragments make up most of the other components, along with a few percent total of olivine, pyroxene, and hornblende. Surprisingly, little evidence of volcanic glass or palagonite (its alteration product) could be found. Apparently, most of the ash consists of pre-existing fluvial sands that were incorporated into tuffs during steam-charge eruptions. (See: Arvidson and Mutch, 1974)

6-Volcanic Tuff-2: The sample is from a fluvial deposit collected from the middle of the floor of MacDougal Crater in the Pinacates volcanic field, sieved to utilize the 177 to 250 μm size fraction. The sample is much like #5, although with a slightly larger component of olivine, and a few percent of what appear to be a mixture of clay minerals and iron hydroxides.

7-Volcanic Tuff-3: The sample consists of crushed cinders from the fluvial deposits on the floor of MacDougal crater in the Pinacates volcanic field. The size fraction used was the 177-250 μm interval. The crushed cinders consist of intergrowths of plagioclase feldspar, olivine, clinopyroxene, opaque minerals, and glass. The intent of using samples 5, 6, and 7 was to characterize: (a) the in-situ tuff deposits (#5), (b) the cinder component (#7), and (c) thoroughly weathered materials from the crater floor (#6).

8-Volcanic Tuff-4: This sample is a fluvial sediment collected from the floor of Sykes crater, Pinacates. Size interval used is 177-250 μm. About 60% of the sample consists of rock fragments of fine-grained pyroxene, olivine, and feldspar set in a matrix of glass and palagonite. Some phenocrysts of olivine, feldspar, and dolomite are present.

C. Following is a listing of positively identified minerals in the samples, together with ideal compositions. Minerals with iron, a transition metal, show significant absorption features between the UV and near IR, as can be seen from Appendix III.

MINERAL	IDEAL COMPOSITION
Limonite	$Fe_2O_3 \cdot nH_2O$
Hypersthene	$(Mg, Fe)\ SiO_3$
Augite	$Ca(Mg,Fe,Al)\ (Al,Si)_2O_6$

MINERAL	IDEAL COMPOSITION
Olivine	$(Mg,Fe)_2SiO_4$
Potash feldspar	$K\ Al\ Si_3O_8$
Plagioclase feldspar	$(Na,Ca)\ (Al,Si)Al\ Si_2O_8$
Quartz	SiO_2
Dolomite	$(Ca,Mg)\ (CO_3)_2$

APPENDIX II: PHOTOGRAPHS OF SAMPLES TAKEN WITH A QUASI-MICROSCOPE AND WITH A HIGH-QUALITY PETROGRAPHIC MICROSCOPE

A. The samples discussed in Appendix I were photographed with reflected light using the breadboard quasi-microscope attached to the FID Viking-like camera. Eight broad band, high resolution views were obtained, and in addition, samples 1, 2, 3, and 4 were photographed in color. All samples were then photographed in black and white and in color with a Zeiss microscope utilizing reflected light. Unfortunately, it was not possible to photograph the exact same fields of view with the quasi-microscope and the Zeiss set-up. Nonetheless, comparison of the photographs is highly instructive, since the Zeiss provides a resolving power of about 3 μm at 50% MTF, while the quasi-microscope high resolution view has about an 11 μm pixel size, and in the multispectral mode the pixel size is about 33 μm. In effect, the Zeiss photographs provide a ground truth with which to test the utility of the quasi-microscope to characterize samples.

B. Following are black and white and color photographs, with brief figure captions. The black and white QM views are the broad band or high resolution views.

Figure II-1: Black and white views of sample #7 - volcanic tuff-3.

In this figure and in the following figures, the quasi-microscope (QM) photograph is the circular one. The diameter of the field of view is about 4mm. For the Zeiss photograph, the field of view is somewhat under 2 mm. The Zeiss view shows subangular grains, some bright, some dark, that are partially covered with small spall zones, which probably formed during crushing of the rock. The spall zones give rise to the specular reflectance. Such detail is lost on the QM photograph, although the overall shape and angularity of the grains can be discerned. Illumination was at near normal incidence.

Figure II-2: Color views of sample #7 - volcanic tuff-3.

The Zeiss color view provides a great deal of information, much more so than the equilvalent black and white view. In particular, translucent to greenish-brown opaque grains can be seen, implying quartz-feldspar minerals to pyroxene -

hornblende - olivine kinds of minerals. The transparent grains are quartz, while the reddish grains are potash feldspar. Spall zones visible in Figure II-1 are subdued in the color Zeiss view because illumination was kept at about 45^{0} from vertical. The QM color view provides little to no information on grain surface texture. The distribution of grain abundances and color is, however, fairly well characterized.

Figure II-3: Black and white views of sample #2 - basalt.
The Zeiss and QM views provide, in this case, roughly the same kinds of information. In particular, the platy, elongate nature of the dark minerals is well displayed. Illumination is near-normal incidence, with the Zeiss view showing spall pits due to crushing.

Figure II-4: Color views of sample #2 - basalt.

The QM view actually provides a better indication of the distribution of grain types by color than does the Zeiss view. In particular, the white grains are feldspars, the greenish grains are augite fragments,and the golden-brownish grains are hypersthene fragments.

Figure II-5: Black and white views of sample #3 - peridotite.

These views and those in Figure II-6 were taken with illumination at a near normal incidence angle. The peridotite consists of augite, olivine, and hypersthene, although positive identification of these minerals is difficult in either view. The Zeiss photograph does show several fragments that are platy, elongate, and dark, suggesting a pyroxene-like cleavage. Such information is not as obvious in the QM view.

Figure II-6: Color views of sample #3 - peridotite.

Many of the dark grains are underexposed, unfortunately, in the Zeiss view. The black vertical and horizontal stripe on the QM photograph is part of a grid pattern on the background material. The distribution of color is a useful characterization on the QM photograph, although individual grains cannot be resolved.

Figure II-7: Black and white views of sample #4 - limonite.

The QM image suggests that the sample is an aggregate of grains. That observation is clearly evident on the Zeiss view.

Figure II-8: Color views of sample #4-limonite

The distinctive yellowish-brown color of limonite is well-displayed on both views. On the Zeiss view, but not on the QM view, a number of grains of what appear to be quartz or feldspar can be seen. Such information cannot be seen on the QM view because the relatively low resolving power precludes seeing the semi-specular reflectance from cleavage and fracture surfaces.

Figure II-9, 10, 11, 12: Black and white views of sample #1-latite, #5-tuff-1, #6-tuff-2, and #8-tuff-4.

In all four sets of views, more surface texture is evident on the Zeiss view, although both sets of views fairly well characterize the size, shape, and roundness of the grains. The high frequency roundness component is subdued to some extent on the QM views. Also, small spall zones due to crushing on sample #1, in particular, are impossible to recognize on the QM view. The increase in dark, mafic (Fe, Mg) bearing from #5, as opposed to #1, is evident from both sets of views.

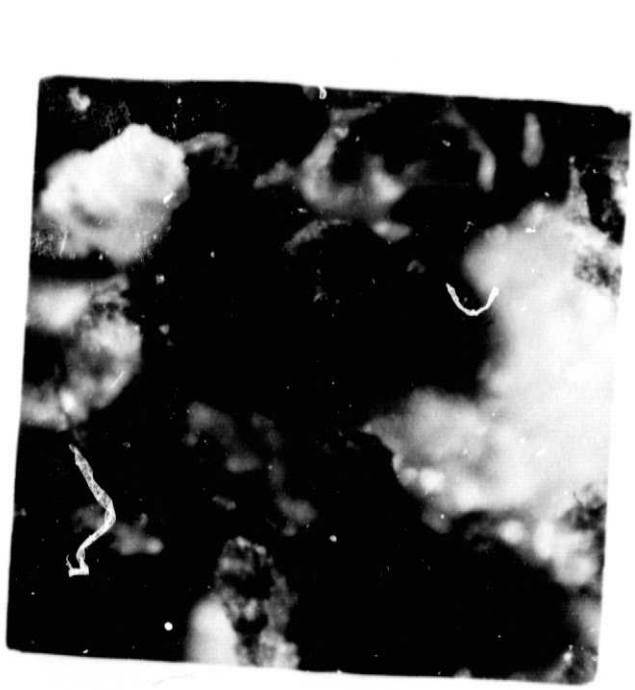

Figure II-1:
Sample #7-volcanic tuff #3

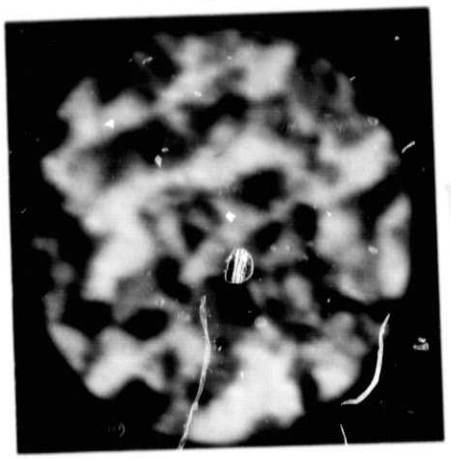

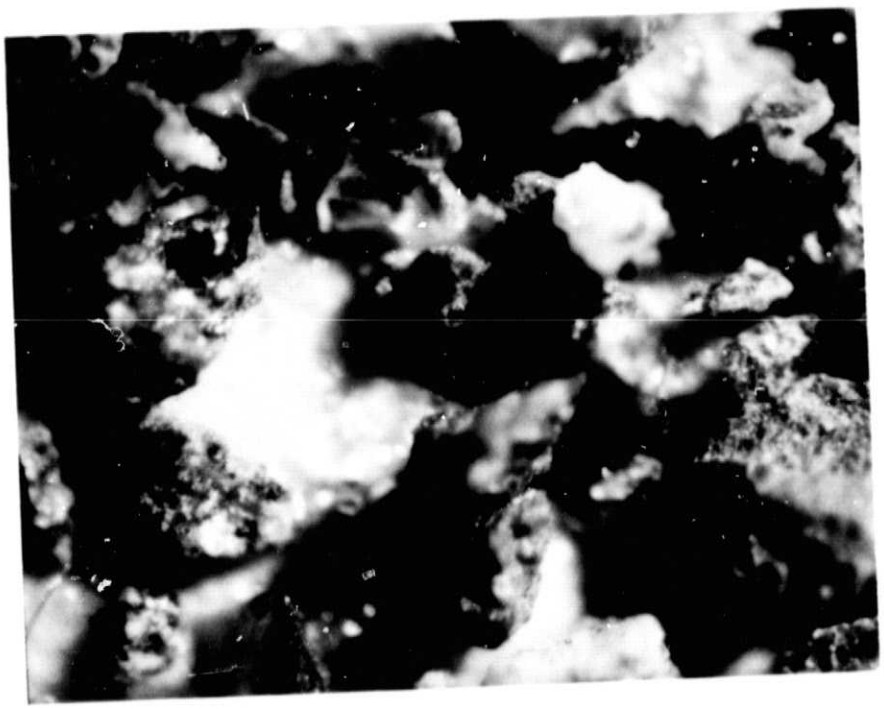

Figure II-2:

Sample #7-volcanic tuff #3

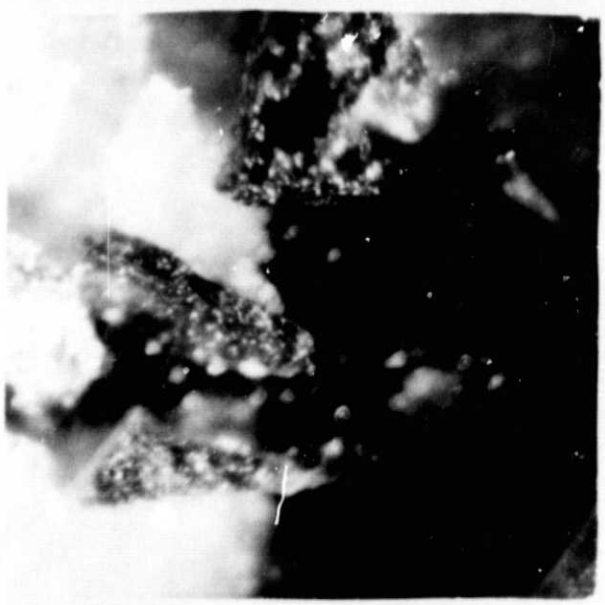

Figure II-3:

Sample #2-basalt

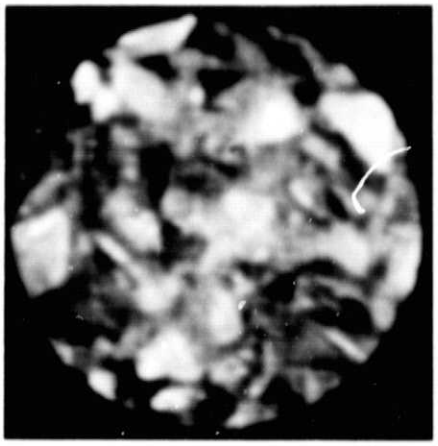

Figure II-4:

Sample #2-basalt

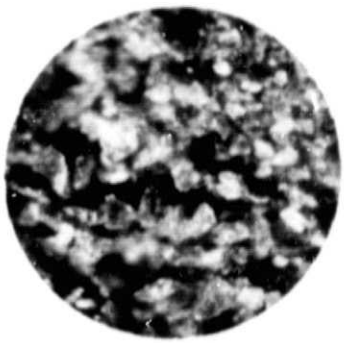

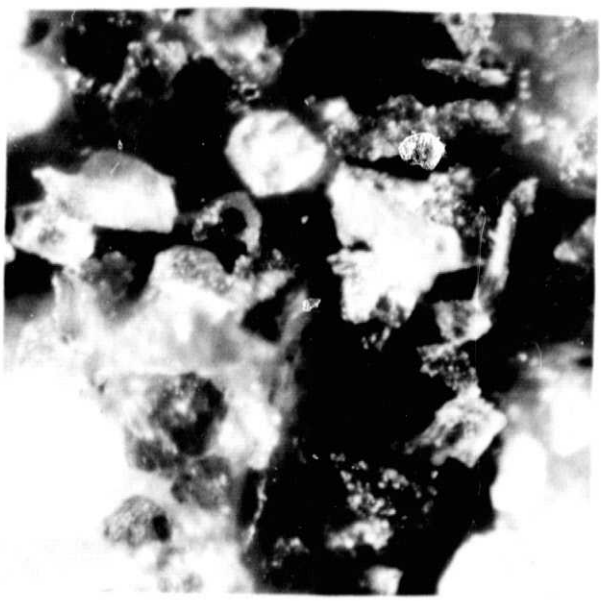

Figure II-5:

Sample #3-peridotite

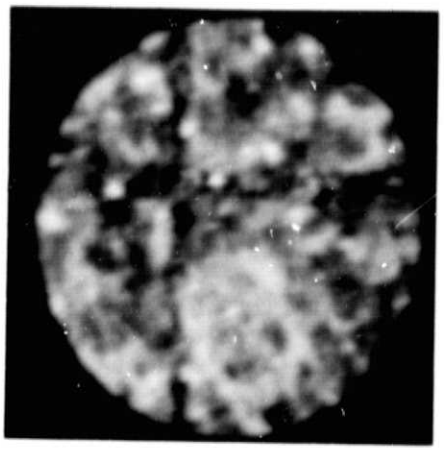

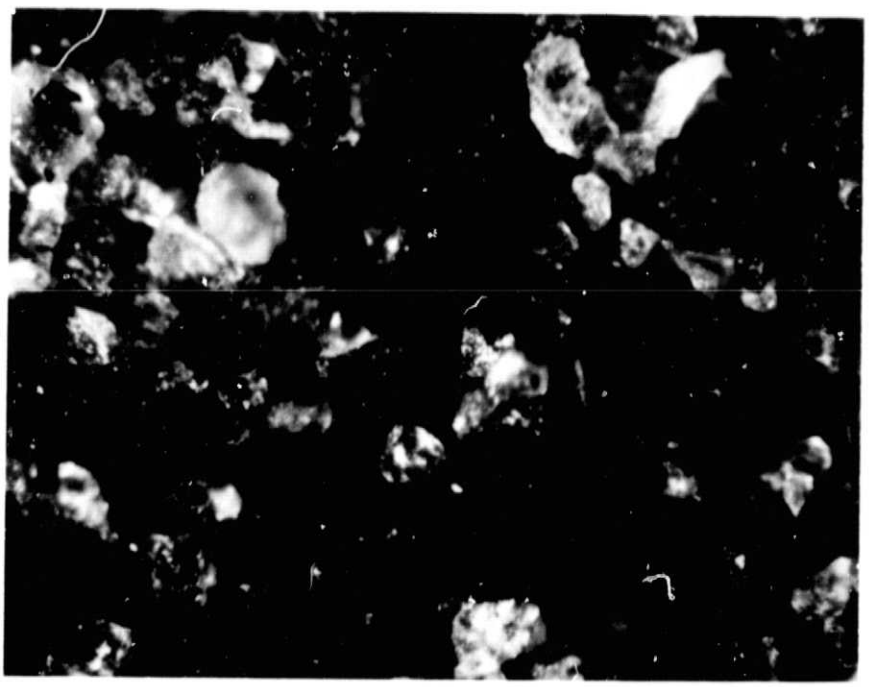

Figure II-6:

Sample #3-peridotite

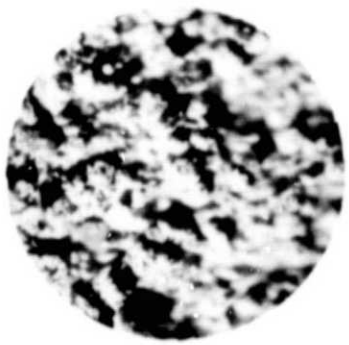

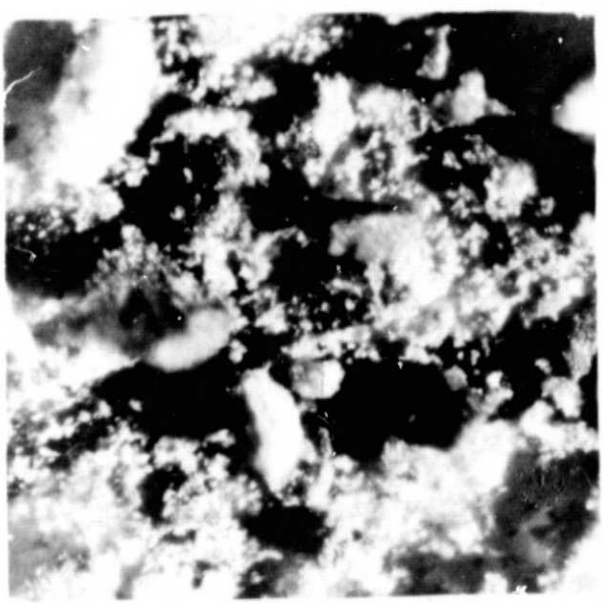

Figure II-7:

Sample #4-limonite

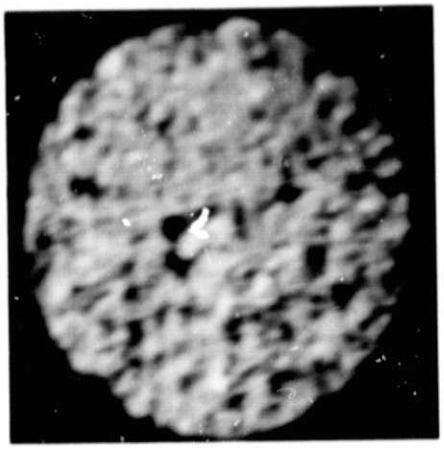

Figure II-8:

Sample #4-limonite

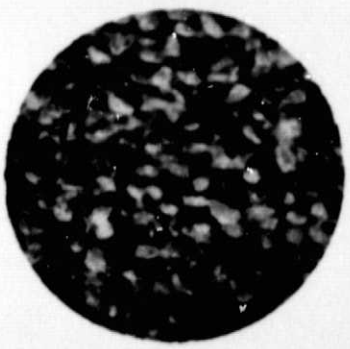

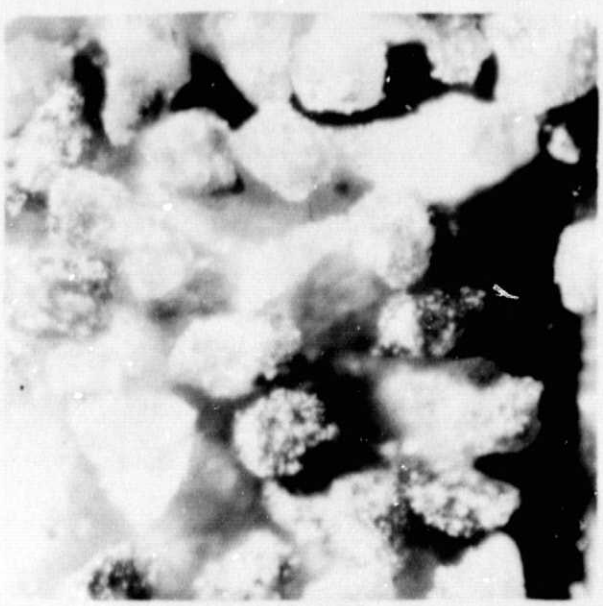

Figure II-9:

Sample #1-latite

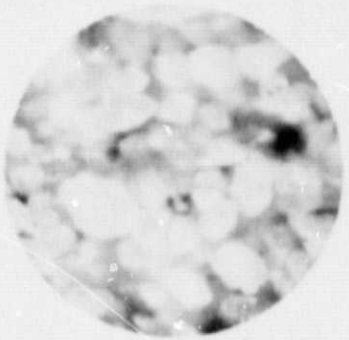

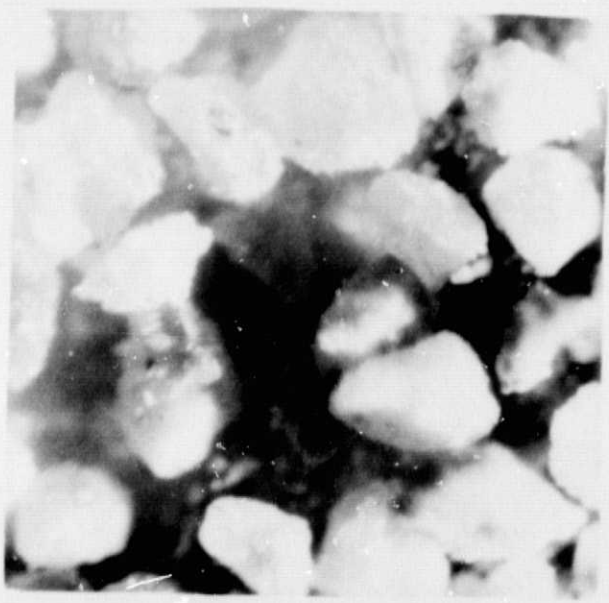

Figure II-10:

Sample #5-volcanic tuff #1

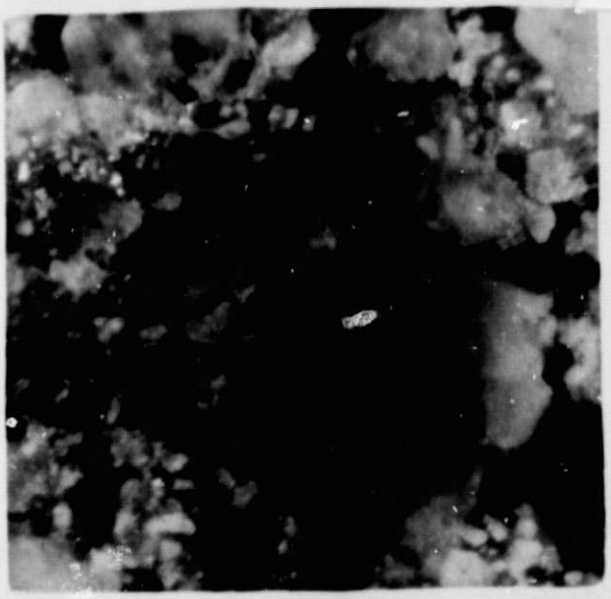

Figure II-11:

Sample #6-volcanic tuff #2

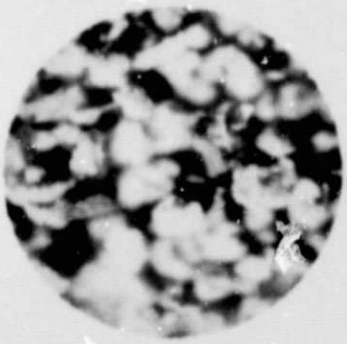

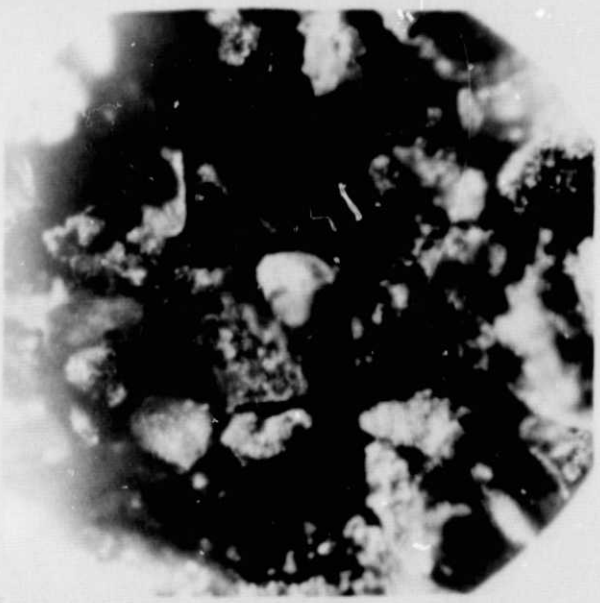

Figure II-12:

Sample #8-volcanic tuff #4

APPENDIX III: LIBRARY OF SPECTRAL REFLECTANCES (.4-1.1 μm) FOR SAMPLES USED IN VARIOUS PHASES OF RESEARCH

A. Following are tabular and graphical displays of the spectral reflectances of a number of samples run using the Langley FID Cary 14 Recording Spectrophotometer. Samples were crushed, if needed, and placed in glass containers. A reference "gray" material, $MgCO_3$, was also powdered and placed in an identical container. The sample and reference containers were placed against the Cary 14 integrating sphere portholes and data were collected for wavelengths from .4 to 1.1 μm simultaneously for the sample and the $MgCO_3$ reference. The sample data were reduced by normalization to the $MgCO_3$ data.

B. Figure Captions for Graphs:

Figure III-1: Samples imaged by both the quasi-microscope and the Zeiss microscope are displayed on these curves. Note the slight absorption centered at about 0.93 μm for the basalt, and the slight absorption at 0.96 μm for the peridotite. The shift in absorption maximum probably reflects the dominance of Fe^{+2} bound in hypersthene and augite for the basalt (which produce electronic transition absorptions at 0.90 μm and 0.95 μm, respectively) as opposed to the dominance of augite and olivine (Fe^{+2} transition absorption around 1.03 - 1.05 μm) in the peridotite. For limonite, the shape of the curve is dominated by an Fe^{+3} electron transition band centered at 0.89 μm. Significant absorptions for many materials occur in the UV, for a number of reasons (Burns and Vaughan, 1975). The right-wing of the UV bands is what produces color in the visible. Note that materials lacking in transition metals, like Fe, do not usually have significant UV absorption.

Samples 5-8 represent increasing content of darker mafic (Fe, Mg) minerals. None of the samples is dominated by pyroxene or olivine to the point of producing significant absorptions near 1.0 μm.

Figure III-2: Samples 9-11 represent finer to coarser grained crushed hypersthene. Hypersthene can have an Fe^{+2} electronic transition band centered at 0.90 μm which does not show in these samples. Neither does the 0.95 μm band show in a distinctive way for the augite. One possible explanation for their absence is that in hand specimen these materials were slightly coated with a yellowish-brown alteration product, which may serve to obscure the true spectra. Samples 13 - 15 represent increasing grain size for olivine samples. Absorptions in the

near-IR are significant. The absorption centered at 1.05 μm is indicative of the electronic transition band due to Fe^{+2} in iron-rich olivine.

Figure III-3 and III-4: For completeness, spectral curves for rhyolite (feldspar, quartz, hornblende-volcanic rock), andesite (feldspar, hornblende, pyroxene, quartz, volcanic rock), obsidian (volcanic glass of basaltic composition), loess (quartz, feldspar, calcite), quartzose sand (quartz, feldspar, hornblende), anhydrite ($CaSO_4$) and montmorillonite (clay mineral), are shown. Note that with the exception of loess, sandstone, and montmorillonite, the spectra are either flat or nearly so. The limestone monotonically increases in reflectance with increasing wavelength. The loess and sandstone both have grains somewhat covered with Fe-rich alteration products - limonite and clay minerals, while the montmorillonite is probably iron-rich. Results demonstrate the need for a transition metal, like iron, to produce significant absorption in the UV, visible, and IR. The feldspars, samples 16-19, are relatively featureless due to the absence of transition metal ions. Samples 17, 18, and 19 represent progressively larger size fractions of anorthite. Ilmenite, $FeTiO_3$, is a poor reflector, with any observable features (e.g.~0.8 μm) probably due to Fe^{+3} transitions. Although obsidian is iron-rich, absorption is minimized because the iron does not occupy the proper location in a crystal lattice for significant absorptions in the wavelength range under consideration.

TABLE III - 1
Reflectance values for samples imaged by the quasimicroscope.
Numbers below sample name indicate grain size fraction used.

WAVELENGTH, MICRONS	1-LATITE 74-250μ	2-BASALT 177-500μ	3-PERIDOTITE 74-250μ	4-LIMONITE 74-250μ	5-VOLCANIC TUFF-1 177-500μ	6-VOLCANIC TUFF-2 177-500μ	7-VOLCANIC TUFF-3 177-500μ	8-VOLCANIC TUFF-4 177-500μ
.400	.098	.091	.089	.036	.091	.095	.088	.054
.425	.104	.098	.091	.042	.110	.108	.094	.060
.450	.117	.110	.093	.050	.123	.126	.101	.060
.475	.123	.110	.099	.056	.135	.139	.097	.073
.500	.130	.117	.099	.068	.154	.152	.104	.098
.525	.138	.119	.112	.094	.175	.166	.111	.104
.550	.145	.126	.119	.144	.201	.186	.111	.124
.575	.157	.126	.119	.195	.226	.211	.117	.137
.600	.170	.126	.120	.215	.252	.231	.118	.150
.625	.170	.126	.120	.228	.264	.242	.118	.161
.650	.170	.119	.113	.233	.270	.250	.124	.175
.675	.169	.112	.113	.233	.281	.262	.130	.188
.700	.169	.119	.114	.253	.288	.267	.130	.199
.725	.168	.112	.113	.277	.292	.272	.130	.216
.750	.173	.111	.112	.286	.296	.274	.130	.232
.775	.177	.104	.116	.282	.299	.279	.125	.248
.800	.176	.097	.114	.275	.303	.280	.123	.256
.825	.175	.096	.113	.256	.301	.284	.123	.266
.850	.177	.091	.108	.241	.304	.284	.123	.278
.875	.173	.086	.104	.232	.302	.285	.124	.291
.900	.171	.090	.100	.238	.304	.284	.119	.302
.925	.167	.090	.094	.226	.308	.288	.120	.312
.950	.168	.090	.089	.228	.310	.293	.123	.331
.975	.168	.090	.089	.234	.310	.289	.117	.333
1.000	.173	.090	.089	.240	.308	.288	.117	.344
1.025	.171	.101	.088	.252	.310	.281	.117	.350
1.050	.163	.100	.088	.258	.306	.275	.115	.350
1.075	.163	.106	.088	.275	.306	.281	.106	.362
1.100	.170	.113	.094	.294	.308	.275	.106	.362

TABLE III - 2

Reflectance values for selected minerals.
Numbers below sample names indicate grain size fraction used.

WAVE-LENGTH-MICRONS	9-HYPER-STHENE <75μ	10-HYPER-STHENE 75-250μ	11-HYPER-STHENE 250-1180μ	12-AUGITE 177-500μ	13-OLIV-INE <75μ	14-OLIV-INE 75-250μ	15-OLIV-INE 250-1180μ	16-LABRA-DORITE 177-500μ	17-ANOR-THITE <75μ	18-ANOR-THITE 75-250μ	19-ANOR-THITE 250-1180μ	20-ILMEN-ITE 177-500μ
.400	.202	.098	.054	.071	.294	.218	.175	.310	.215	.239	.163	.060
.425	.202	.098	.055	.084	.301	.256	.213	.311	.356	.245	.189	.054
.450	.209	.104	.056	.084	.325	.282	.247	.311	.374	.258	.204	.054
.475	.209	.111	.056	.091	.405	.333	.284	.315	.393	.270	.216	.054
.500	.222	.111	.056	.091	.414	.389	.333	.317	.420	.284	.228	.055
.525	.228	.111	.056	.098	.457	.432	.381	.319	.432	.290	.238	.049
.550	.230	.117	.056	.106	.491	.469	.419	.323	.441	.304	.244	.050
.575	.238	.123	.056	.099	.506	.472	.419	.323	.462	.312	.244	.050
.600	.238	.125	.056	.094	.519	.472	.400	.331	.462	.319	.244	.050
.625	.244	.126	.051	.093	.519	.450	.378	.329	.469	.325	.250	.050
.650	.250	.126	.044	.087	.512	.438	.361	.325	.469	.325	.247	.050
.675	.248	.131	.050	.081	.509	.435	.350	.325	.472	.323	.244	.050
.700	.250	.138	.050	.074	.512	.428	.323	.323	.475	.325	.236	.050
.725	.269	.137	.056	.074	.512	.407	.286	.331	.475	.325	.236	.049
.750	.262	.137	.049	.067	.506	.383	.245	.329	.488	.326	.233	.049
.775	.273	.136	.055	.067	.509	.352	.220	.333	.484	.329	.232	.048
.800	.270	.140	.060	.065	.503	.341	.187	.333	.485	.331	.229	.048
.825	.268	.146	.054	.065	.500	.289	.157	.331	.482	.329	.229	.059
.850	.273	.145	.054	.065	.485	.270	.137	.331	.479	.327	.214	.059
.875	.267	.146	.055	.067	.461	.256	.122	.333	.473	.315	.220	.061
.900	.264	.146	.050	.068	.448	.238	.112	.333	.466	.307	.217	.062
.925	.259	.142	.051	.062	.432	.225	.101	.325	.457	.302	.222	.062
.950	.262	.138	.052	.064	.431	.208	.077	.331	.450	.300	.219	.057
.975	.262	.139	.058	.069	.425	.195	.071	.321	.450	.294	.221	.057
1.000	.264	.139	.052	.062	.428	.174	.058	.325	.440	.289	.221	.056
1.025	.264	.139	.052	.062	.428	.162	.052	.325	.440	.289	.208	.056
1.050	.266	.139	.052	.062	.430	.157	.045	.325	.443	.291	.208	.056
1.075	.278	.139	.045	.062	.430	.164	.045	.325	.443	.291	.201	.050
1.100	.278	.139	.045	.062	.437	.164	.052	.325	.449	.291	.208	.044

TABLE III - 3

Reflectance spectra for selected igneous rocks.
Numbers below samples refer to grain size fractions used.

WAVELENGTH MICRONS	21-RHYOLITE < 75μ	22-RHYOLITE 75-250μ	23-RHYOLITE 250-1180μ	24-ANDESITE <75μ	25-ANDESITE 75-250μ	26-ANDESITE 250-1180μ	27-OBSIDIAN <75μ	28-OBSIDIAN 75-250μ	29-OBSIDIAN 250-1180μ
.400	.546	.374	.235	.344	.264	.193	.491	.282	.120
.425	.522	.378	.244	.344	.270	.207	.491	.286	.122
.450	.509	.380	.259	.344	.276	.246	.497	.288	.130
.475	.509	.388	.259	.356	.288	.228	.503	.290	.130
.500	.512	.388	.259	.370	.296	.241	.512	.290	.123
.525	.531	.395	.262	.370	.309	.250	.512	.290	.125
.550	.534	.395	.262	.373	.317	.256	.516	.290	.125
.575	.538	.407	.269	.381	.325	.262	.519	.290	.125
.600	.544	.418	.275	.381	.331	.262	.519	.294	.125
.625	.550	.428	.288	.381	.338	.269	.519	.256	.128
.650	.562	.428	.291	.381	.338	.266	.525	.302	.133
.675	.565	.431	.294	.379	.335	.262	.522	.300	.131
.700	.575	.438	.292	.381	.338	.261	.525	.300	.124
.725	.588	.441	.298	.381	.338	.261	.538	.298	.124
.750	.594	.447	.301	.381	.338	.258	.538	.298	.129
.775	.602	.457	.305	.385	.342	.256	.540	.302	.122
.800	.607	.457	.301	.380	.344	.265	.534	.299	.126
.825	.610	.463	.301	.390	.354	.265	.530	.299	.120
.850	.606	.461	.292	.388	.352	.262	.527	.297	.113
.875	.606	.457	.299	.388	.352	.268	.521	.293	.116
.900	.595	.451	.298	.380	.356	.267	.522	.280	.112
.925	.593	.451	.297	.383	.352	.266	.512	.272	.108
.950	.600	.450	.303	.381	.344	.271	.512	.269	.103
.975	.600	.456	.299	.388	.350	.273	.500	.266	.104
1.000	.585	.449	.292	.389	.352	.273	.503	.266	.104
1.025	.585	.449	.292	.389	.352	.266	.497	.259	.097
1.050	.582	.443	.286	.392	.354	.266	.494	.253	.084
1.075	.582	.443	.279	.390	.354	.260	.494	.247	.078
1.100	.582	.443	.273	.390	.354	.260	.481	.247	.078

TABLE III - 4

Reflectance spectra for selected sedimentary materials.
Numbers below sample names refer to grain size fraction used.

WAVELENGTH, MICRONS	30-LOESS 177-500μ	31-QUARTZOSE SAND 74-250μ	32-LIMESTONE 74-250μ	33-ANHYDRITE <75μ	34-ANHYDRITE 75-250μ	35-ANHYDRITE 250-1180μ	36-MONTMO-RILLONITE <75μ	37-MONTMO-RILLONITE 75-250μ	38-MONTMO-RILLONITE 250-1180μ
.400	.095	.143	.185	.650	.497	.337	.098	.074	.024
.425	.114	.170	.201	.650	.515	.366	.098	.073	.043
.450	.126	.199	.211	.644	.540	.407	.110	.092	.062
.475	.158	.211	.217	.650	.558	.426	.135	.111	.068
.500	.171	.224	.224	.654	.574	.438	.148	.123	.080
.525	.196	.256	.231	.654	.580	.450	.185	.148	.100
.550	.224	.288	.238	.658	.584	.456	.224	.173	.125
.575	.248	.302	.245	.662	.588	.456	.269	.210	.150
.600	.269	.323	.259	.662	.594	.462	.306	.238	.169
.625	.280	.323	.259	.662	.600	.494	.325	.258	.179
.650	.294	.321	.270	.669	.612	.506	.344	.270	.184
.675	.300	.327	.277	.665	.615	.512	.354	.275	.188
.700	.311	.335	.285	.675	.625	.528	.369	.281	.186
.725	.321	.333	.289	.681	.631	.540	.375	.292	.186
.750	.335	.335	.298	.681	.638	.528	.381	.298	.190
.775	.345	.344	.301	.683	.640	.543	.398	.309	.189
.800	.351	.347	.311	.681	.638	.536	.399	.311	.193
.825	.355	.345	.315	.683	.646	.542	.402	.317	.190
.850	.355	.349	.325	.679	.642	.536	.406	.315	.190
.875	.364	.348	.338	.673	.636	.536	.406	.311	.189
.900	.370	.350	.338	.675	.638	.540	.405	.305	.186
.925	.369	.346	.340	.673	.630	.544	.401	.309	.184
.950	.376	.354	.348	.675	.625	.548	.400	.306	.187
.975	.377	.361	.354	.669	.625	.552	.400	.304	.182
1.000	.381	.367	.361	.667	.629	.545	.402	304	.182
1.025	.388	.365	.365	.667	.629	.545	.402	.310	.182
1.050	.388	.371	.377	.671	.627	.545	.411	.310	.180
1.075	.394	.369	.375	.665	.627	.545	.418	.316	.180
1.100	.400	.369	.388	.665	.633	.545	.430	.323	.182

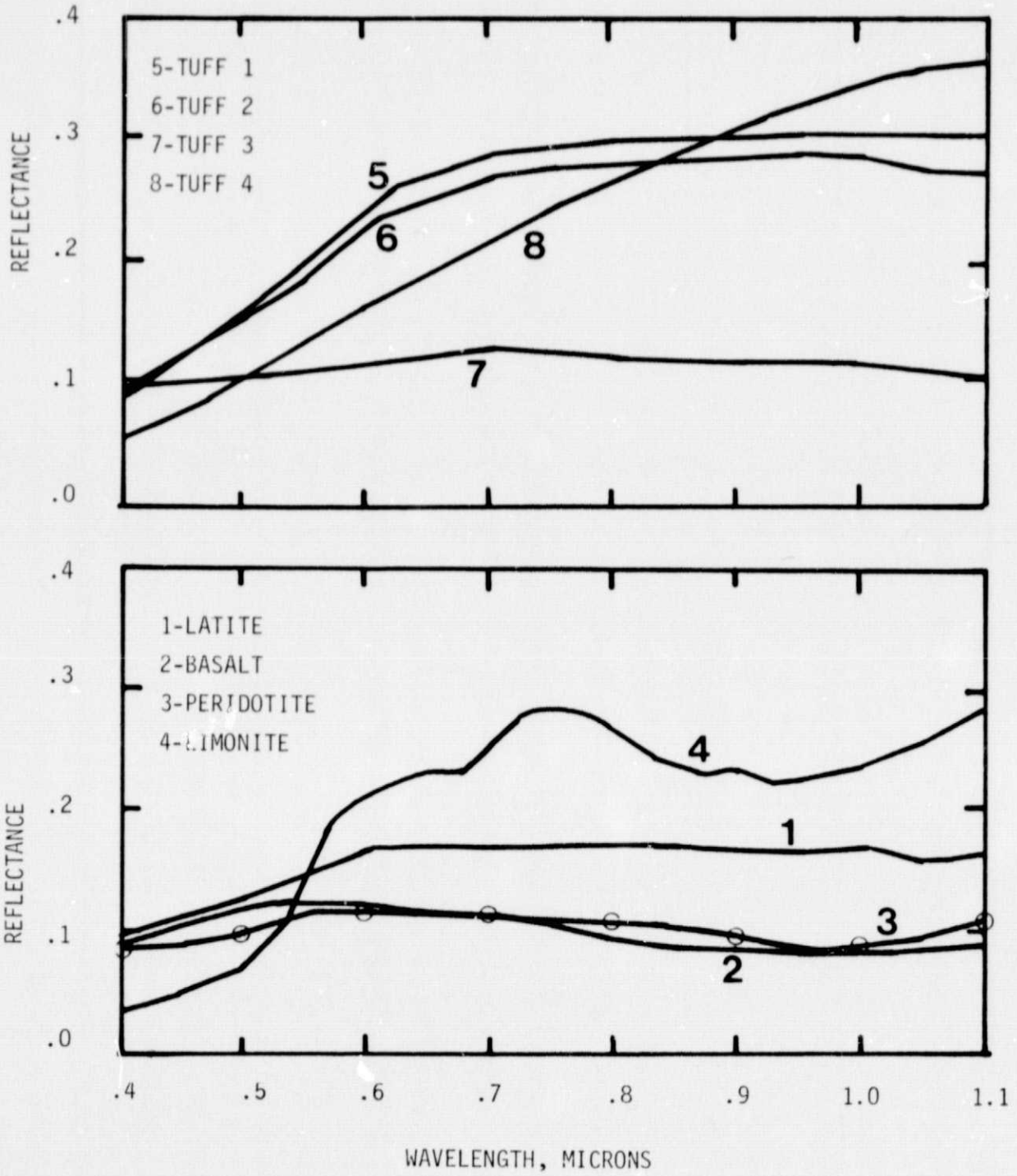

Figure III-1

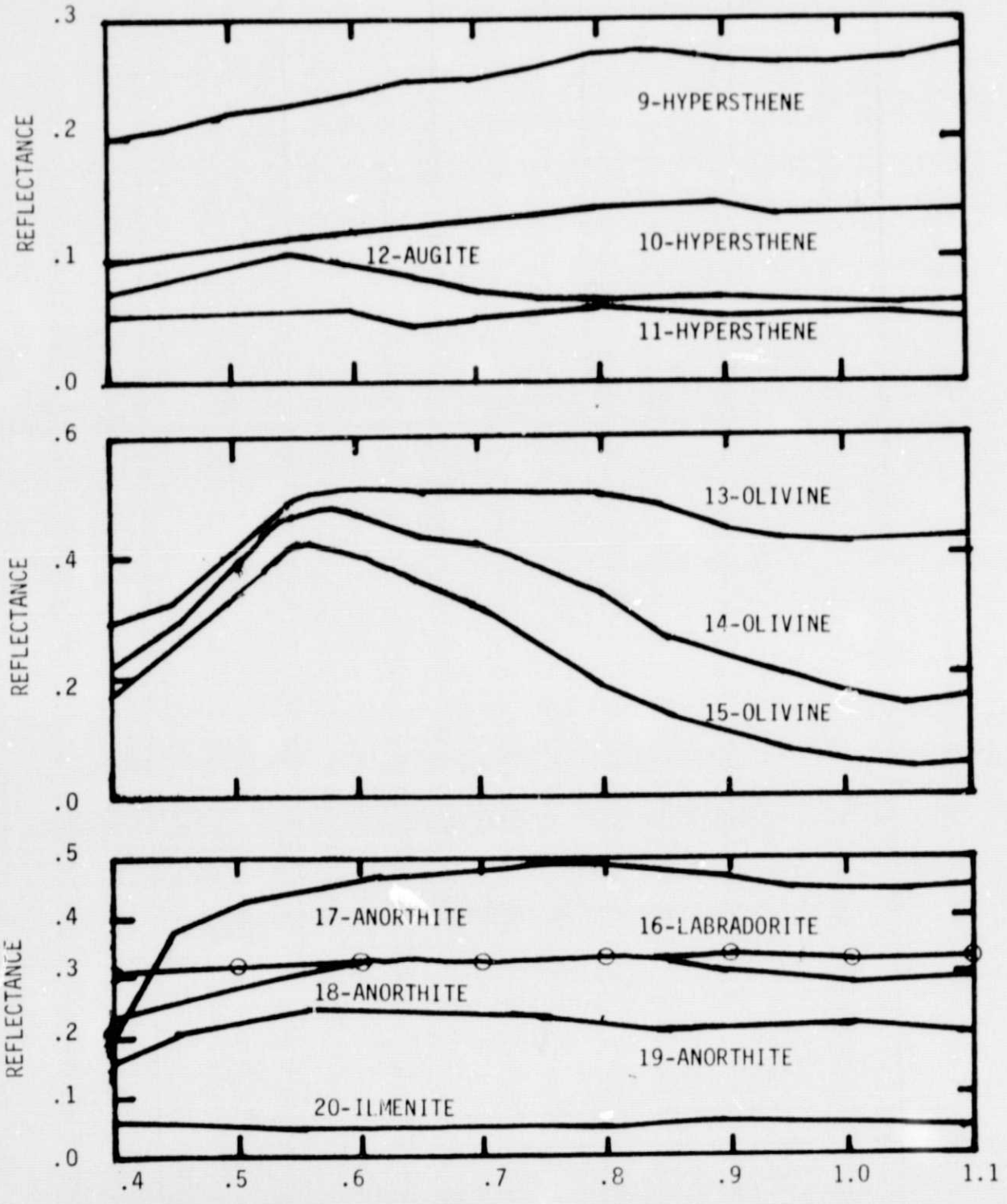
REFLECTANCE
.3
.2
.1
.0
9-HYPERSTHENE
10-HYPERSTHENE
12-AUGITE
11-HYPERSTHENE
REFLECTANCE
.6
.4
.2
.0
13-OLIVINE
14-OLIVINE
15-OLIVINE
REFLECTANCE
.5
.4
.3
.2
.1
.0
17-ANORTHITE
16-LABRADORITE
18-ANORTHITE
19-ANORTHITE
20-ILMENITE
.4
.5
.6
.7
.8
.9
1.0
1.1
WAVELENGTHS, MICRONS

Figure III-2

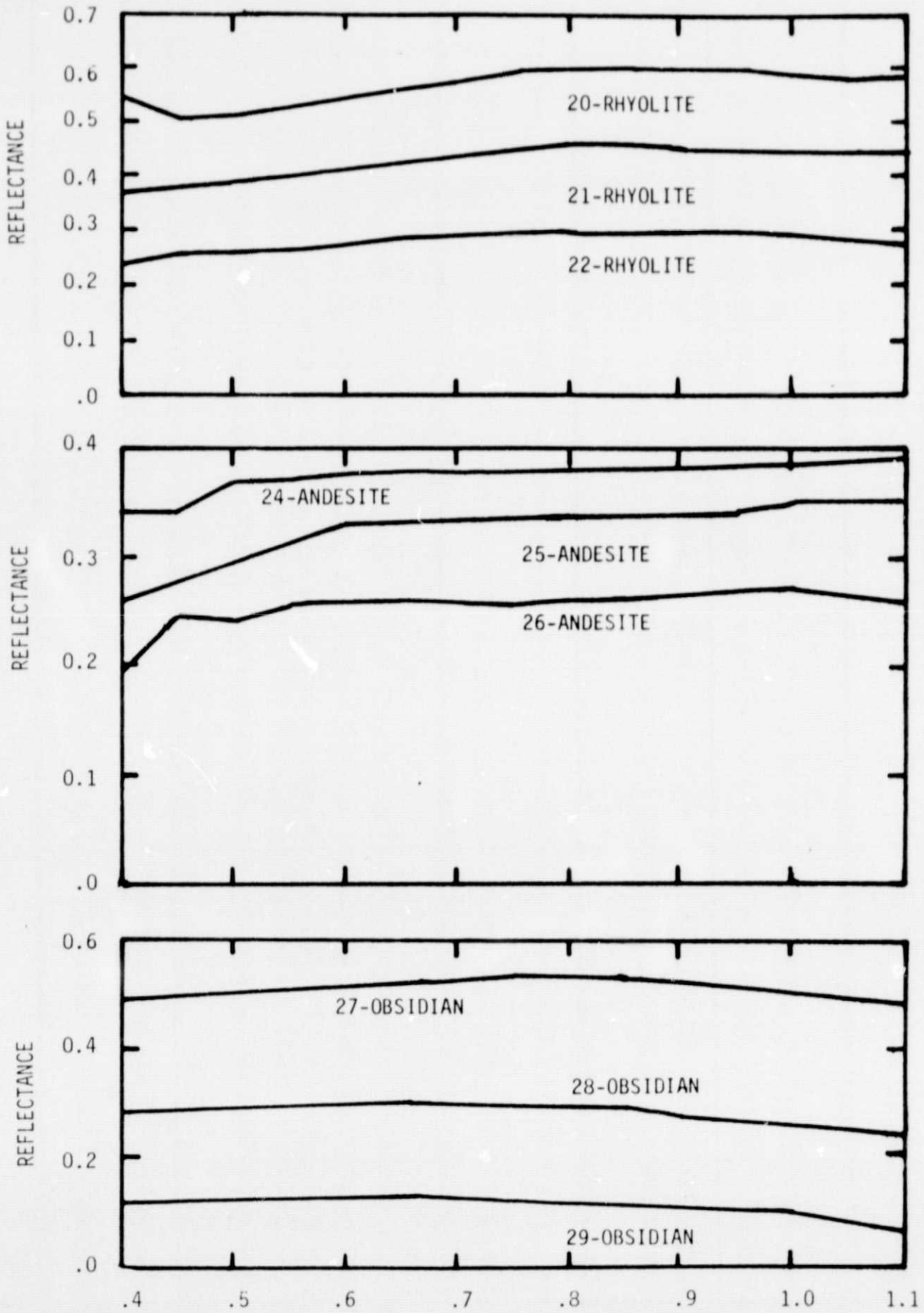

Figure III-3

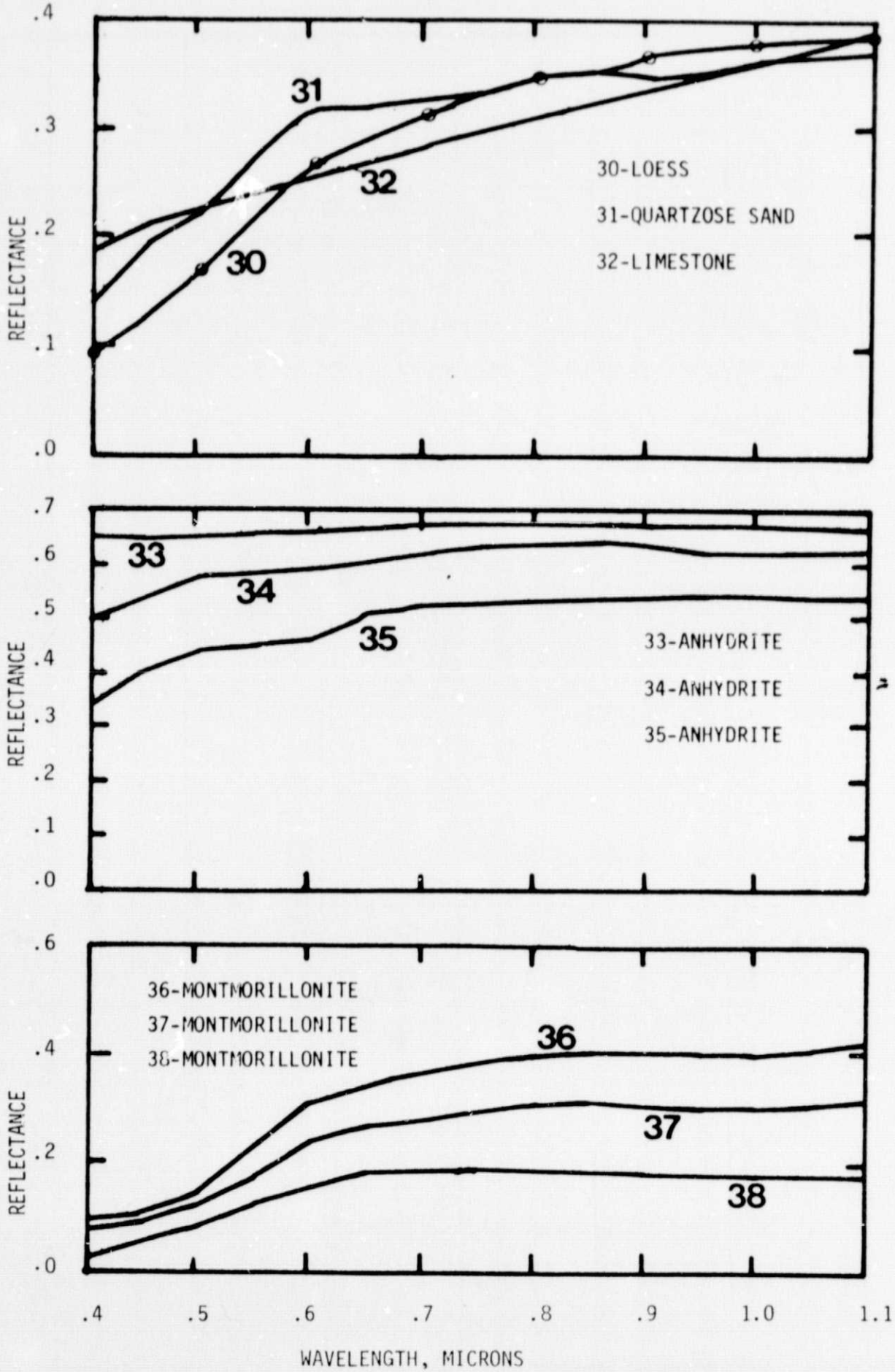
.4
.3
.2
.1
.0
REFLECTANCE
31
32
30
30-LOESS
31-QUARTZOSE SAND
32-LIMESTONE
.7
.6
.5
.4
.3
.2
.1
.0
REFLECTANCE
33
34
35
33-ANHYDRITE
34-ANHYDRITE
35-ANHYDRITE
.6
.4
.2
.0
REFLECTANCE
36-MONTMORILLONITE
37-MONTMORILLONITE
38-MONTMORILLONITE
36
37
38
.4
.5
.6
.7
.8
.9
1.0
1.1
WAVELENGTH, MICRONS

Figure III-4